



# Lanthanum Oxide Nickel Hydroxide Composite Triangle Nanosheets for Energy Density Asymmetric Supercapacitors

Huiyu Duan<sup>†</sup>, Mei Shi<sup>†</sup>, Mengfei Zhang, Geyu Feng, Suli Liu and Changyun Chen\*

Key Laboratory of Advanced Functional Materials of Nanjing, School of Environmental Science, Nanjing Xiaozhuang University, Nanjing, China

## OPEN ACCESS

### Edited by:

Kuaibing Wang,  
Nanjing Agricultural University, China

### Reviewed by:

Yuqiao Wang,  
Southeast University, China  
Xiaoquan Yao,  
Nanjing University of Aeronautics and  
Astronautics, China  
Zhao Bo,  
Nanjing Normal University, China

### \*Correspondence:

Changyun Chen  
cychen@njzcu.edu.cn

<sup>†</sup>These authors have contributed  
equally to this work and share first  
authorship

### Specialty section:

This article was submitted to  
Electrochemistry,  
a section of the journal  
Frontiers in Chemistry

Received: 27 September 2021

Accepted: 18 October 2021

Published: 11 November 2021

### Citation:

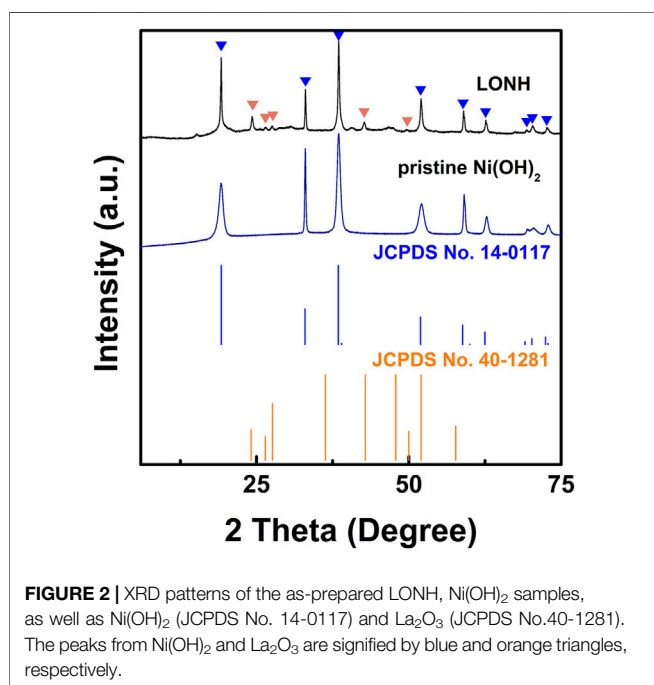
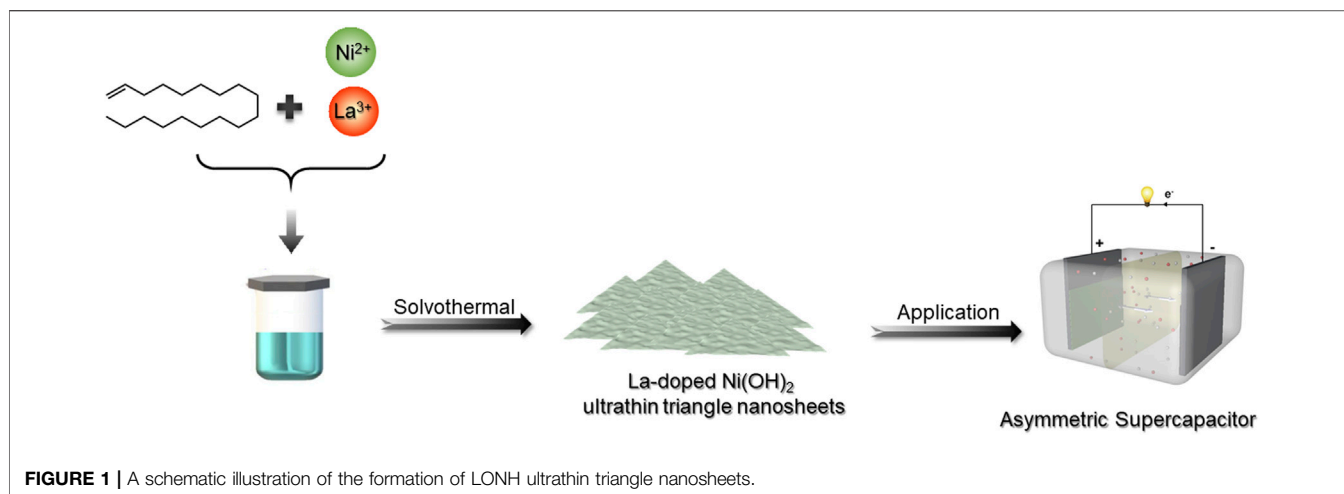
Duan H, Shi M, Zhang M, Feng G, Liu S  
and Chen C (2021) Lanthanum Oxide  
Nickel Hydroxide Composite Triangle  
Nanosheets for Energy Density  
Asymmetric Supercapacitors.  
Front. Chem. 9:783942.  
doi: 10.3389/fchem.2021.783942

Transition metal hydroxides are a kind of promising electrode material in electrochemical energy storage, but the poor conductivity limits their application. Lanthanides are good proton conductors and can usually improve the intrinsic conductivity of other materials. By integrating the merits of lanthanide elements and transition metal hydroxide, we designed lanthanum oxide nickel hydroxide composites (LONH) with unique ultrathin triangle nanosheet morphology via a controllable synthetic strategy for high-performance supercapacitors. When the LONH is used as positive electrode material in aqueous asymmetric supercapacitor, it reveals an energy density ( $107.8 \text{ W h kg}^{-1}$  at  $800 \text{ W kg}^{-1}$ ), rate performance (86.9% retention at  $4 \text{ kW kg}^{-1}$ ) and outstanding cycle stability (more than 90% retention after 3,000 cycles). This work confirms that compositing  $\text{La}_2\text{O}_3$  and  $\text{Ni}(\text{OH})_2$  can significantly improve the supercapacitor performance of both pristine  $\text{La}_2\text{O}_3$  and transition metal hydroxide composites. We hope this work would offer a good prospect for developing other lanthanide-transition metal hydroxide composites as an attractive class of electrode materials in electrochemical energy storage.

**Keywords:** asymmetric supercapacitor, electrochemical energy storage, nanosheet, transition metal hydroxides, rare earth

## INTRODUCTION

Transition metal hydroxides (TMHs) and derivatives have attracted much attention as electrode materials for application in electrocatalysis (Gong et al., 2013; Fan et al., 2014; Han et al., 2016; Sun et al., 2018; Liu et al., 2019; Zhang et al., 2021a; Zhang et al., 2021b), electrochemical analysis (Tan et al., 2017), and especially electrochemical energy storage (Chen et al., 2014; Zuo et al., 2016; Yao et al., 2018; Jiang et al., 2019; Zhang et al., 2019, 2019; Wang et al., 2020; Yin et al., 2020, 2020; Gürbüz et al., 2021; Jiang et al., 2021; Song et al., 2021b; Song et al., 2021a; Zhang et al., 2021a). As a critical member of TMHs, nickel hydroxides show great potential for high-performance electrode with much lower cost than novel metal-based materials. Thus, Ni-based hydroxides have become a popular electrode material for electrochemistry (Song et al., 2021b). In addition, Ni-based hydroxides usually possess good Faradic activity, which means they are suitable for electrochemical energy storage. There are many meaningful works about Ni-based hydroxides applied for electrochemical energy storage. For example, Zhang et al. reported  $\text{Co}(\text{CO}_3)_{0.5}(\text{OH})/\text{Ni}_2(\text{CO}_3)(\text{OH})_2$  nanobelts as positive electrode materials for flexible asymmetric supercapacitor, displaying a high energy density of  $22.7 \text{ Wh kg}^{-1}$  at a power density of  $24,019 \text{ W kg}^{-1}$  (Zhang et al., 2020). Chen et al. reported single

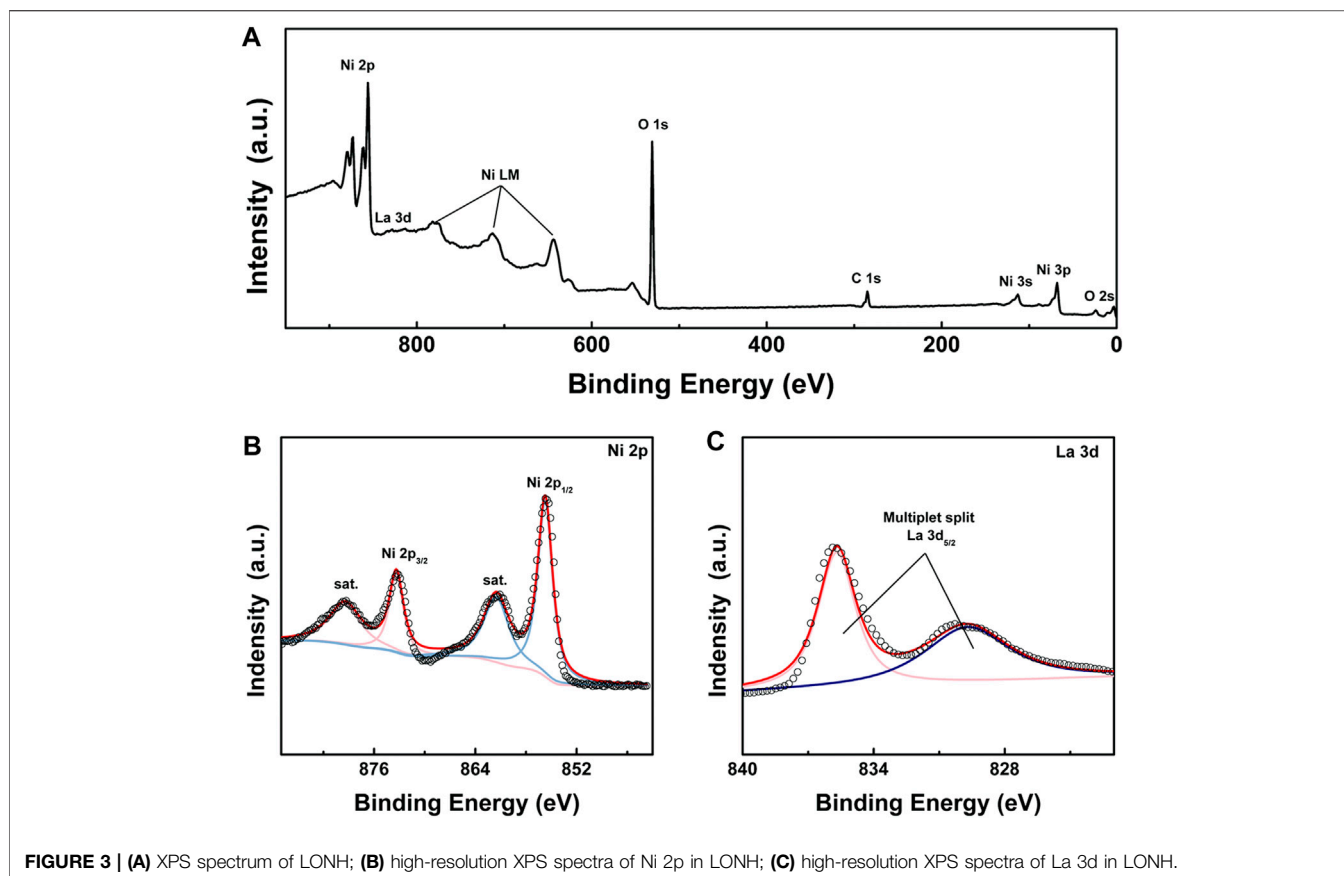


crystalline  $\beta$ -Ni(OH)<sub>2</sub> quasi-nanocubes used for aqueous Ni-Zn batteries, exhibiting high areal energy and power density (Chen et al., 2021). However, the poor electrical and ionic conductivity of Ni-based hydroxides restricts their many applications in electrochemistry. Thermal treatment can convert hydroxides to oxides, which is a good approach to improve the conductivity, but this process is usually accompanied by layer collapse and structural change, leading to the attenuation of capacitance.

Lanthanide compounds have been widely utilized in many fields (e.g., photocatalysis, photoelectrocatalysis, bioimage) because of the singular optical properties (Liu et al., 2011; Zhou et al., 2015; Escudero-Escribano et al., 2016; Han et al., 2017; Hosseinpour-Mashkani and Sobhani-Nasab, 2017; Regmi et al., 2017; Li et al., 2019). Additionally, most lanthanide compounds are good proton conductors, which can enhance

the ion and electron conductivity of electrode materials composited in it (Duan et al., 2019; Ghosh et al., 2019; Duan et al., 2020; Rabani et al., 2021). In our previous works, we found that the addition of lanthanide elements can significantly influence morphology, thickness, and electrochemical properties. In one case, Yb was introduced in Ni(OH)<sub>2</sub> to obtain Ni<sub>4</sub>Yb(OH)<sub>10</sub>NO<sub>3</sub>·3H<sub>2</sub>O hexagonal nanosheets (Zhu et al., 2021). After addition of Yb, there was significant reduction in thickness of Ni(OH)<sub>2</sub> nanosheets. When used as electrode material for supercapacitor, the nanosheets showed high capacity that was over 3 times of pristine Ni(OH)<sub>2</sub>. Because it is easier for Yb<sup>3+</sup> to devote charges to a conductive carrier from the shell 4f<sup>13</sup> of the Yb<sup>3+</sup> path and because of reduction in thickness, the electron and ion transport routes were both shortened, resulting in better electrical and ionic conductivity. La, as the representative element of lanthanides, possesses most of the typical properties of lanthanide elements. When added into transition metal-based materials, it can enhance the electrochemical performance. For example, Chakrabarty et al. by La doping enhanced the electrochemical performance of Ni(OH)<sub>2</sub>/carbon nanotube hybrid electrodes. Despite the fact that the hybrid electrodes show high capacitance (2,731 F g<sup>-1</sup> at 1 A g<sup>-1</sup>), the energy density (~25 Wh kg<sup>-1</sup> at ~1 kW kg<sup>-1</sup>) is unsatisfactory because of the low charge voltage.

In our study of lanthanide elements and Ni-based hydroxide composites, we found that the addition of lanthanum can change the morphology of Ni(OH)<sub>2</sub> to ultrathin triangle nanosheets and also significantly boost the supercapacitor performance. In this work, a facile method was used to synthesize lanthanum oxide nickel hydroxide composites (LONH) triangle nanosheets, and they were used as electrode materials for supercapacitors. The LONH triangle nanosheets present an outstanding specific capacitance (783.0 F g<sup>-1</sup> at 1 A g<sup>-1</sup>), which is about double that of pristine Ni(OH)<sub>2</sub>. Moreover, an aqueous asymmetric supercapacitor (ASC) was assembled with LONH, exhibiting a very high energy density, up to 107.8 Wh kg<sup>-1</sup> at 800 W kg<sup>-1</sup>. This synthetic strategy can also expand to the reliable production of other lanthanide-TMH composites, and we hope it can boost the improvement of electrochemical energy storage.



## RESULTS AND DISCUSSION

The fabrication of LONH is schematically shown in **Figure 1** via a facile method (Supporting Information shows the more synthetic details). X-ray diffraction (XRD) characterized the structure of LONH (**Figure 2**). The pattern demonstrates that the LONH consists of Ni(OH)<sub>2</sub> (JCPDS No. 14-0117) and La<sub>2</sub>O<sub>3</sub> (JCPDS No.40-1281). There are eight peaks (signed by blue triangles) corresponding to the (001), (100), (101), (102), (110), (111), (103), and (201) facets of Ni(OH)<sub>2</sub>, respectively. Four peaks (signified by orange triangles) correspond to the (100), (002), (101), and (110) facets of La<sub>2</sub>O<sub>3</sub>.

The element composition and chemical state of LONH were examined by X-ray photoelectron spectroscopy (XPS). **Figure 3A** presents the survey spectrum, demonstrating that Ni, La, O, C, and a little N are evident. **Figure 3B** is the Ni 2p high-resolution spectrum, revealing two peaks from Ni 2p<sub>1/2</sub> and Ni 2p<sub>3/2</sub> signals of Ni(II) at 855.7 and 873.2 eV accompanying the satellite peaks at 861.3 and 879.4 eV. **Figure 3C** shows the two peaks at 830.5 and 835.2 eV, in accordance with multiplet split La 3d<sub>5/2</sub>. The  $\Delta E$  of multiplet split La 3d<sub>5/2</sub> is 4.9 eV, which indicates that the existence form of La is La<sub>2</sub>O<sub>3</sub>, corresponding to the result of XRD analysis.

Transmission electron microscopy (TEM) was used to disclose the morphological features of pristine Ni(OH)<sub>2</sub>, La<sub>2</sub>O<sub>3</sub>, and LONH. According to **Figure 4A**, pristine Ni(OH)<sub>2</sub> possesses a heavily aggregated multiple layer structure. **Figure 4B** shows the

morphology of pristine La<sub>2</sub>O<sub>3</sub>, demonstrating the nanorod-like structure. Interestingly, once La is added into Ni(OH)<sub>2</sub> in the form of La<sub>2</sub>O<sub>3</sub>, the morphology of Ni(OH)<sub>2</sub> will significantly change. As shown in **Figure 4C**, unlike pristine Ni(OH)<sub>2</sub> and La<sub>2</sub>O<sub>3</sub>, LONH consists of unique dispersed ultrathin triangle nanosheets. High-resolution transmission electron microscopy (HRTEM) was used to further study the phase composition of LONH in **Figure 4D**. There are two main interplanar spacings of 0.35 and 0.46 nm, corresponding to (100) facet of La<sub>2</sub>O<sub>3</sub> and (001) facet of Ni(OH)<sub>2</sub>, respectively, and in good agreement with the main peaks of La<sub>2</sub>O<sub>3</sub> and Ni(OH)<sub>2</sub> in the XRD pattern. **Figures 4E–H** show the element mapping images of La, Ni, and O in LONH, indicating that La, Ni, and O are uniformly distributed in LONH nanosheets.

Cyclic voltammetry (CV) is a necessary method in electrochemistry to figure out the redox behavior of LONH. **Supplementary Figure S1** shows the CV curves at different scan rates from 10 to 50 mV s<sup>-1</sup> in electrolyte of 3 M KOH. The CV curves indicate that the redox behavior of LONH mainly consists of Ni(OH)<sub>2</sub>, with the existence of OH<sup>-</sup>. The large area enclosed by CV curves indicates the outstanding Faradic process, which results in an excellent pseudocapacitive performance. The integrate method was used to calculate the capacity of LONH from CV curves, indicating that the specific capacities of LONH are 889.4, 881.0, 852.0, 813.1, and 780.7 F g<sup>-1</sup> at 1.0–5.0 A g<sup>-1</sup>.

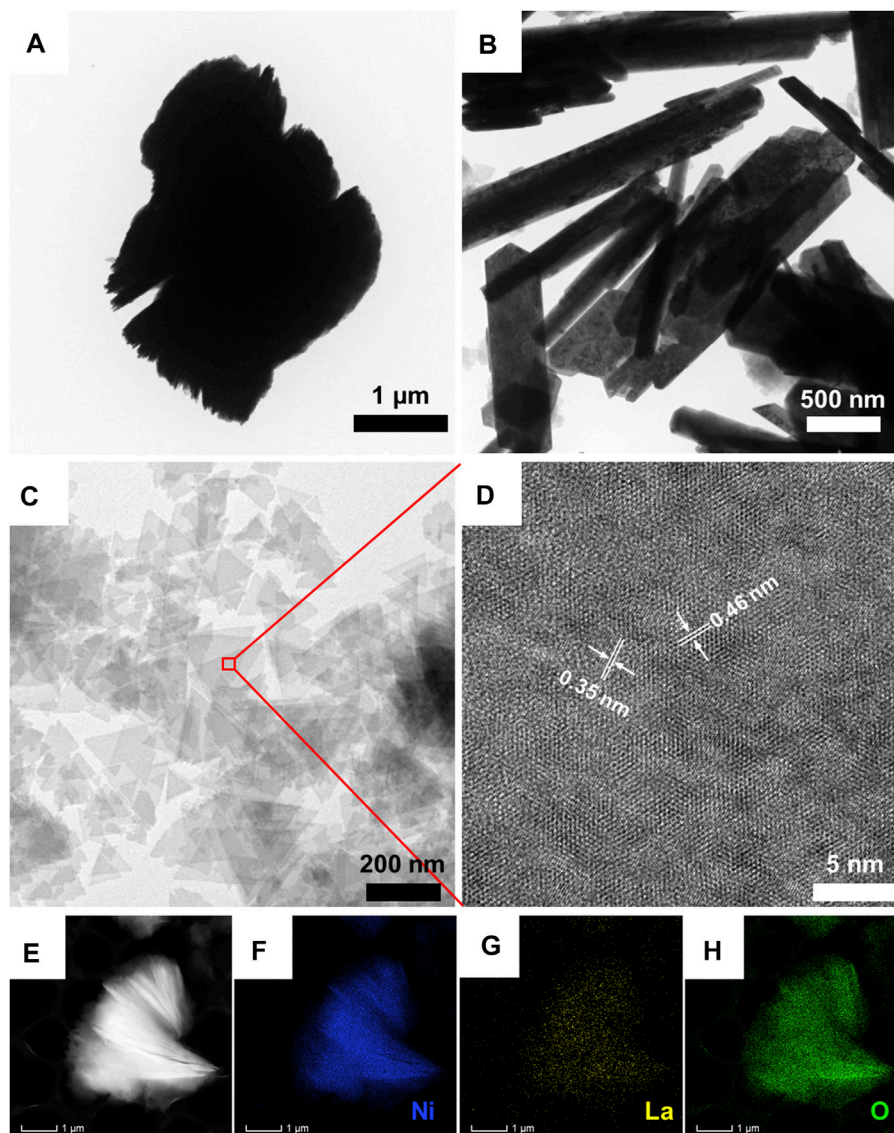
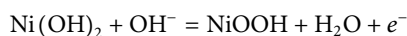


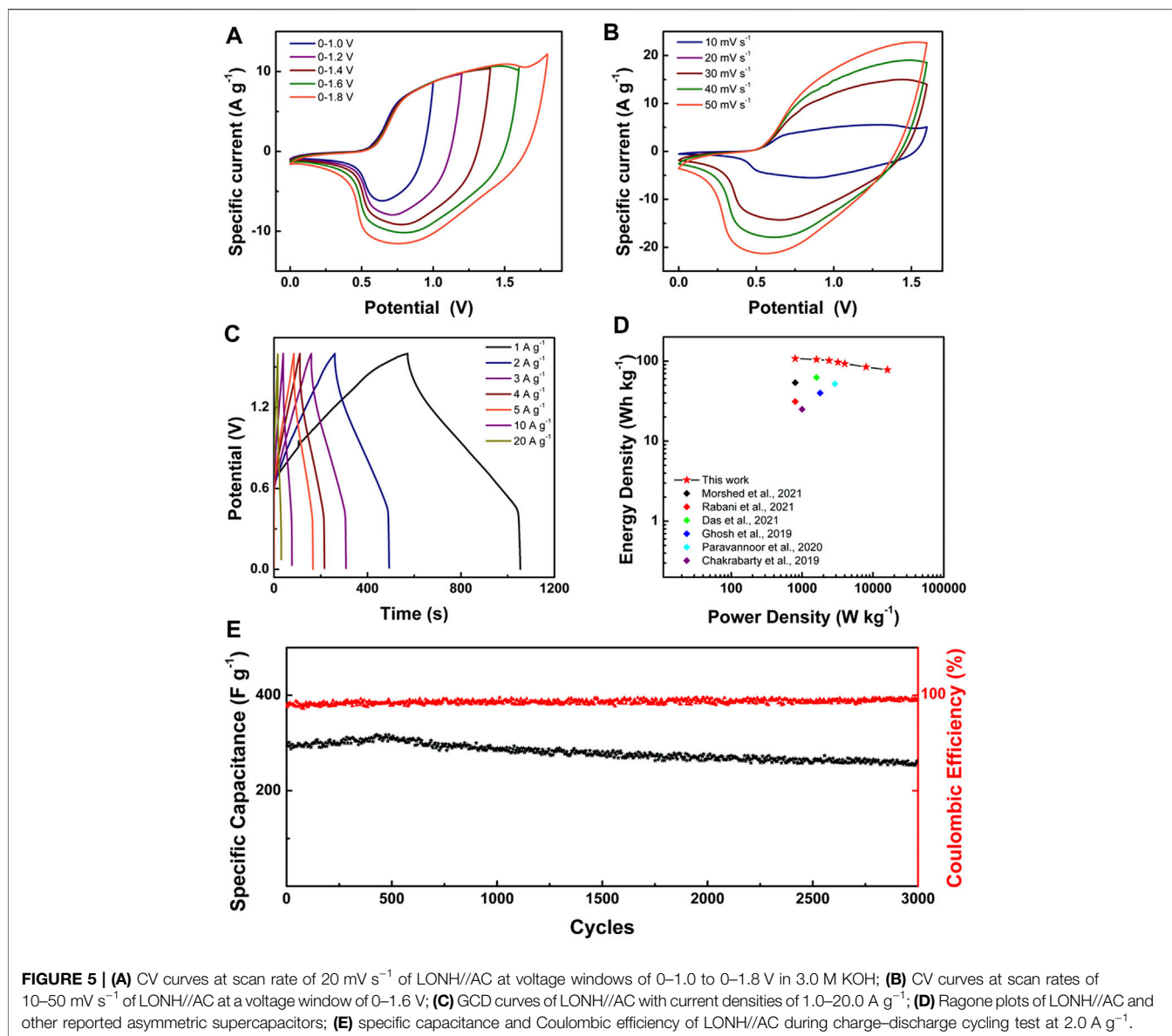
**FIGURE 4 |** TEM images of (A) pristine Ni(OH)<sub>2</sub>, (B) pristine La<sub>2</sub>O<sub>3</sub>, and (C) LONH; (D) HRTEM image of LONH; (E–H) energy dispersive spectroscopy (EDS) mapping images of LONH.



The galvanostatic charge–discharge (GCD) was used to investigate the specific capacitance of LONH. **Supplementary Figure S2** shows the GCD curves within a voltage window of 0.15–0.55 V at different current densities of 1.0–5.0 A g<sup>-1</sup>, in which the platforms confirm the presence of redox processes, corresponding to the CV results. In line with the GCD curves, the specific capacitance of LONH was calculated to be 783.0, 717.5, 659.3, 631.8, and 616.3 F g<sup>-1</sup> at current densities of 1.0–5.0 A g<sup>-1</sup>, respectively. **Supplementary Figure S3** exhibits the capacitances of LONH in different current densities to investigate the rate performance (78.7% retention at 5.0 A g<sup>-1</sup>). To compare the capacitance of LONH and pristine Ni(OH)<sub>2</sub>, their GCD curves are shown in **Supplementary Figure S4**, revealing that the

capacitance of LONH is about double that of pristine Ni(OH)<sub>2</sub>. It demonstrates that the addition of La can obviously enhance the energy storage performance of pristine Ni(OH)<sub>2</sub>.

For practice application, we assembled an aqueous ASC device in which the positive electrode used LONH and the negative electrode used activated carbon (AC), respectively (denoted as LONH//AC). The CV (**Supplementary Figure S5**) and GCD (**Supplementary Figure S6**) measurements were applied on AC, revealing that the specific capacity of AC is 86.3 F g<sup>-1</sup> at 1.0 A g<sup>-1</sup>. Because the specific capacity of LONH is 783.0 F g<sup>-1</sup> at 1.0 A g<sup>-1</sup>, to balance the charge during charging and discharging, the ratio of LONH and AC is about 1:8.8. In order to figure out the suitable voltage window of LONH//AC, CV analysis results with different voltage windows of 0–1.0, 0–1.2, 0–1.4, 0–1.6, and 0–1.8 V are



shown in **Figure 5A**. When the charging voltage is above 1.6 V, obvious electrolyte decomposition occurs, indicating that the most suitable voltage window is 0–1.6 V. The CV and GCD curves of LONH//AC at divergent scan rates were shown in **Figures 5B,C**. The LONH//AC reaches an energy density of 107.8 W h kg<sup>-1</sup> at 800 W kg<sup>-1</sup> and exhibits outstanding rate performance of 86.9% retention at 4 kW kg<sup>-1</sup>. Even at a power density of 16 kW kg<sup>-1</sup>, it still remains 77.8 W h kg<sup>-1</sup>, benefited from the shortened electron and ion transport routes in LONH nanosheets. According to the above test results, LONH//AC is significantly better than previously reported ASCs (**Supplementary Table S1**), such as PANI/La-10 (56.1 W h kg<sup>-1</sup> at 400 W kg<sup>-1</sup>) (Morshed et al., 2021), Ce-MOF-0.5//AC (31.3 W h kg<sup>-1</sup> at 800 W kg<sup>-1</sup>) (Rabani et al., 2021), NiV-LDH (2:2)//Bi<sub>2</sub>O<sub>3</sub> (65.5 W h kg<sup>-1</sup> at 1,595.2 W kg<sup>-1</sup>) (Das et al., 2021), MOF-Ce (40 W h kg<sup>-1</sup> at

1,800 W kg<sup>-1</sup>) (Ghosh et al., 2019), PrO<sub>x</sub>/CNT//V<sub>2</sub>O<sub>5</sub>/graphene (52.1 W h kg<sup>-1</sup> at 2,900 W kg<sup>-1</sup>) (Paravannoor et al., 2020), and La-Ni(OH)<sub>2</sub>/MWCNT (25 W h kg<sup>-1</sup> at 1,000 W kg<sup>-1</sup>) (Chakrabarty and Chakraborty, 2019). **Figure 5D** shows the corresponding comparison Ragone plot.

It is critical for these devices to work reliably and stably for a long time. **Figure 5E** displays the cycling stability result of LONH//AC via continuously charging and discharging at 2.0 A g<sup>-1</sup>. In the 1st cycle, the capacitance of LONH//AC was 294.1 F g<sup>-1</sup>. With cycle number increasing, the capacitance constantly grew and reached the maximum of 317.3 F g<sup>-1</sup> at about the 400th cycle. After cycling 1,000 times, the capacitance declined to 286.6 F g<sup>-1</sup>. With continuing cycles, the rate decreased. It finally declined to 262.4 F g<sup>-1</sup> after 3,000 cycles, and still retained about 90% of its initial capacity. The Coulombic efficiency increased from 89.6 to 96.1% during the whole 3,000 cycles, indicating the good

reversibility. For comparison, the cycling stability results of Ni(OH)<sub>2</sub>//AC, La<sub>2</sub>O<sub>3</sub>//AC, and LONH//AC are shown in **Supplementary Figure S7**, which reveals that the capacity retention of Ni(OH)<sub>2</sub>//AC is 63.8% after 2,000 cycles. After ~300 cycles, the capacity of La<sub>2</sub>O<sub>3</sub>//AC decreased to 0 quickly, demonstrating that the addition of La<sub>2</sub>O<sub>3</sub> to Ni(OH)<sub>2</sub> can enhance the capacity and cycle stability.

## CONCLUSION

In conclusion, lanthanide elements and TMH composites are attractive electrode materials for electrochemical energy storage. In this work, we designed the composite LONH with unique ultrathin triangle nanosheets from lanthanide elements and TMHs. With regard to LONH, not only Ni(OH)<sub>2</sub> can ensure high pseudo-capacitance arising from the abundant redox active sites but also the addition of La can make Ni(OH)<sub>2</sub> much more thinner to significantly shorten ion and electron transport pathways. CV and GCD measurements demonstrate that LONH possesses good redox activity and presents an outstanding specific capacity of 783.0 F g<sup>-1</sup> at 1 A g<sup>-1</sup>. Furthermore, the ASC device (LONH//AC) shows an energy density of 107.8 W h kg<sup>-1</sup> at a power density of 800 W kg<sup>-1</sup> and retains 86.9% at 4 kW kg<sup>-1</sup>. According to the result of stability test, LONH//AC shows the capacitance of 262.4 F g<sup>-1</sup> after 3,000 cycles (90.1% retention of the first cycle) and high Coulombic efficiency of 96.1%. This work infers that the addition of lanthanide oxides to Ni(OH)<sub>2</sub> can significantly change the morphology and improve the electrochemical energy storage performance of pristine TMHs. We hope this work would provide an inspiration to develop other lanthanide-TMH

## REFERENCES

- Chakrabarty, N., and Chakraborty, A. K. (2019). Controlling the Electrochemical Performance of β-Ni(OH)<sub>2</sub>/Carbon Nanotube Hybrid Electrodes for Supercapacitor Applications by La Doping: A Systematic Investigation. *Electrochimica Acta* 297, 173–187. doi:10.1016/j.electacta.2018.11.174
- Chen, H., Hu, L., Chen, M., Yan, Y., and Wu, L. (2014). Nickel-Cobalt Layered Double Hydroxide Nanosheets for High-Performance Supercapacitor Electrode Materials. *Adv. Funct. Mater.* 24, 934–942. doi:10.1002/adfm.201301747
- Chen, T., Bai, Y., Xiao, X., and Pang, H. (2021). Exposing (0 0 1) Crystal Facet on the Single Crystalline β-Ni(OH)<sub>2</sub> Quasi-Nanocubes for Aqueous Ni-Zn Batteries. *Chem. Eng. J.* 413, 127523. doi:10.1016/j.cej.2020.127523
- Das, A. K., Pan, U. N., Sharma, V., Kim, N. H., and Lee, J. H. (2021). Nanostructured CeO<sub>2</sub>/NiV-LDH Composite for Energy Storage in Asymmetric Supercapacitor and as Methanol Oxidation Electrocatalyst. *Chem. Eng. J.* 417, 128019. doi:10.1016/j.cej.2020.128019
- Duan, H., Wang, T., Zhuang, J., Liu, S., Shi, M., and Chen, C. (2019). Facile Synthesis of CeO<sub>2</sub>/Ni(OH)<sub>2</sub> Nanosheets and Their Applications for Supercapacitors. *Nanosci. Nanotechnol. Lett.* 11, 384–389. doi:10.1166/nl.2019.2886
- Duan, H., Wang, T., Wu, X., Su, Z., Zhuang, J., Liu, S., et al. (2020). CeO<sub>2</sub> Quantum Dots Doped Ni-Co Hydroxide Nanosheets for Ultrahigh Energy Density Asymmetric Supercapacitors. *Chin. Chem. Lett.* 31, 2330–2332. doi:10.1016/j.ccl.2020.06.001
- Escudero-Escribano, M., Malacrida, P., Hansen, M. H., Vej-Hansen, U. G., Velazquez-Palenzuela, A., Tripkovic, V., et al. (2016). Tuning the Activity of Pt alloy Electrocatalysts by Means of the Lanthanide Contraction. *Science* 352, 73–76. doi:10.1126/science.aad8892
- Fan, G., Li, F., Evans, D. G., and Duan, X. (2014). Catalytic Applications of Layered Double Hydroxides: Recent Advances and Perspectives. *Chem. Soc. Rev.* 43, 7040–7066. doi:10.1039/C4CS00160E
- Ghosh, S., De Adhikari, A., Nath, J., Nayak, G. C., and Nayek, H. P. (2019). Lanthanide (III) Metal-Organic Frameworks: Syntheses, Structures and Supercapacitor Application. *ChemistrySelect* 4, 10624–10631. doi:10.1002/slct.201902614
- Gong, M., Li, Y., Wang, H., Liang, Y., Wu, J. Z., Zhou, J., et al. (2013). An Advanced Ni-Fe Layered Double Hydroxide Electrocatalyst for Water Oxidation. *J. Am. Chem. Soc.* 135, 8452–8455. doi:10.1021/ja4027715
- Gürbüz, E., Grépin, E., Ringuédé, A., Lair, V., and Cassir, M. (2021). Significance of Molten Hydroxides with or Without Molten Carbonates in High-Temperature Electrochemical Devices. *Front. Energ. Res.* 9, 666165. doi:10.3389/fenrg.2021.666165
- Han, L., Dong, S., and Wang, E. (2016). Transition-Metal (Co, Ni, and Fe)-Based Electrocatalysts for the Water Oxidation Reaction. *Adv. Mater.* 28, 9266–9291. doi:10.1002/adma.201602270
- Han, S., Samanta, A., Xie, X., Huang, L., Peng, J., Park, S. J., et al. (2017). Gold and Hairpin DNA Functionalization of Upconversion Nanocrystals for Imaging and *In Vivo* Drug Delivery. *Adv. Mater.* 29, 1700244. doi:10.1002/adma.201700244
- Hosseinpour-Mashkani, S. S., and Sobhani-Nasab, A. (2017). Investigation the Effect of Temperature and Polymeric Capping Agents on the Size and Photocatalytic Properties of NdVO<sub>4</sub> Nanoparticles. *J. Mater. Sci. Mater. Electron.* 28, 16459–16466. doi:10.1007/s10854-017-7557-3

composites as attractive electrode materials for electrochemical energy storage.

## DATA AVAILABILITY STATEMENT

The original contributions presented in the study are included in the article/**Supplementary Material**, further inquiries can be directed to the corresponding author.

## AUTHOR CONTRIBUTIONS

CC and SL conceived and designed the experiments. HD, MS, and GF performed the experiments and analyzed the data. HD and MZ wrote and revised the manuscript. CC, HD, MS, GF, MZ, and SL discussed and supervised the whole project. All the authors revised and checked the draft.

## ACKNOWLEDGMENTS

Key Projects of Basic Science (Natural Science) Research in Colleges and Universities of Jiangsu Province (21KJA150010).

## SUPPLEMENTARY MATERIAL

The Supplementary Material for this article can be found online at: <https://www.frontiersin.org/articles/10.3389/fchem.2021.783942/full#supplementary-material>

- Jiang, H., Sun, W., Li, W., Wang, Z., Zhou, X., Wu, Z., et al. (2019). Facile Synthesis of Novel V<sub>0.13</sub>Mo<sub>0.87</sub>O<sub>2.935</sub> Nanowires with High-Rate Supercapacitive Performance. *Front. Chem.* 7, 595. doi:10.3389/fchem.2019.00595
- Jiang, T., Tong, J., Huang, C., and Wang, Y. (2021). Preparation of Micro Mulberry Leaf-Like CoO@Ni<sub>3</sub>S<sub>2</sub> for a High-Rate Supercapacitor. *Mater. Lett.* 282, 128711. doi:10.1016/j.matlet.2020.128711
- Li, D., Lai, W.-Y., Shen, X., Shao, Q., and Huang, W. (2019). Real-Time Naked-Eye Recognizable Temperature Monitoring Based on Ho<sup>3+</sup> (Or Tm<sup>3+</sup>)-Activated NaYF<sub>4</sub> Upconversion Nanowires via Visual Multicolor Alteration. *Mater. Chem. Front.* 3, 791–795. doi:10.1039/C8QM00608C
- Liu, Q., Sun, Y., Yang, T., Feng, W., Li, C., and Li, F. (2011). Sub-10 Nm Hexagonal Lanthanide-Doped NaLuF<sub>4</sub> Upconversion Nanocrystals for Sensitive Bioimaging *In Vivo*. *J. Am. Chem. Soc.* 133, 17122–17125. doi:10.1021/ja207078s
- Liu, H., Zhao, D., Liu, Y., Hu, P., Wu, X., and Xia, H. (2019). Boosting Energy Storage and Electrocatalytic Performances by Synergizing CoMoO<sub>4</sub>@MoZn<sub>22</sub> Core-Shell Structures. *Chem. Eng. J.* 373, 485–492. doi:10.1016/j.cej.2019.05.066
- Morshed, M., Wang, J., Gao, M., Cong, C., and Wang, Z. (2021). Polyaniline and Rare Earth Metal Oxide Composition: A Distinctive Design Approach for Supercapacitor. *Electrochimica Acta* 370, 137714. doi:10.1016/j.electacta.2021.137714
- Paravannoor, A., Augustine, C. A., and Ponpandian, N. (2020). Rare Earth Nanostructures Based on PrO/CNT Composites as Potential Electrodes for an Asymmetric Pseudocapacitor Cell. *J. Rare Earths* 38, 625–632. doi:10.1016/j.jre.2019.07.017
- Rabani, I., Karuppasamy, K., Vikraman, D., ul haq, Z., Kim, H.-S., and Seo, Y.-S. (2021). Hierarchical Structured Nano-Polyhedrons of CeO<sub>2</sub>@ZIF-8 Composite for High Performance Supercapacitor Applications. *J. Alloys Compd.* 875, 160074. doi:10.1016/j.jallcom.2021.160074
- Regmi, C., Kshetri, Y. K., Ray, S. K., Pandey, R. P., and Lee, S. W. (2017). Utilization of Visible to NIR Light Energy by Yb<sup>3+</sup>, Er<sup>3+</sup> and Tm<sup>3+</sup> Doped BiVO<sub>4</sub> for the Photocatalytic Degradation of Methylene Blue. *Appl. Surf. Sci.* 392, 61–70. doi:10.1016/j.apsusc.2016.09.024
- Song, L., Wang, Q., Ye, X., Yang, F., Wang, L., Wu, Y., et al. (2021a). Sulfide-Fixed Intrinsic Porous NiCoP for Boosting High Capacitance and Long-Term Stability. *ACS Mater. Lett.* 3, 1016–1024. doi:10.1021/acsmaterialslett.1c00282
- Song, L., Zhu, S., Tong, L., Wang, W., Ouyang, C., Xu, F., et al. (2021b). MXene Quantum Dot Rivet Reinforced Ni-Co LDH for Boosting Electrochemical Activity and Cycling Stability. *Mater. Adv.* 2, 5622–5628. doi:10.1039/D1MA00474C
- Sun, S., Zhai, T., Liang, C., Savilov, S. V., and Xia, H. (2018). Boosted Crystalline/amorphous Fe<sub>2</sub>O<sub>3</sub>- $\delta$  Core/Shell Heterostructure for Flexible Solid-State Pseudocapacitors in Large Scale. *Nano Energy* 45, 390–397. doi:10.1016/j.nanoen.2018.01.015
- Tan, C., Cao, X., Wu, X.-J., He, Q., Yang, J., Zhang, X., et al. (2017). Recent Advances in Ultrathin Two-Dimensional Nanomaterials. *Chem. Rev.* 117, 6225–6331. doi:10.1021/acs.chemrev.6b00558
- Wang, W., Jiang, D., Chen, X., Xie, K., Jiang, Y., and Wang, Y. (2020). A Sandwich-Like Nano-Micro LDH-MXene-LDH for High-Performance Supercapacitors. *Appl. Surf. Sci.* 515, 145982. doi:10.1016/j.apsusc.2020.145982
- Yao, L., Cheng, T., Shen, X., Zhang, Y., Lai, W., and Huang, W. (2018). Paper-Based All-Solid-State Flexible Asymmetric Micro-Supercapacitors Fabricated by a Simple Pencil Drawing Methodology. *Chin. Chem. Lett.* 29, 587–591. doi:10.1016/j.ccl.2018.01.007
- Yin, J., Chen, P., Lu, M., Song, L., Zhang, R., Xu, F., et al. (2020). Cu-Doped CoS<sub>2</sub> Polyhedrons with High Catalytic Activity and Long-Term Stability. *Sci. China Mater.* 63, 1337–1344. doi:10.1007/s40843-020-1316-1
- Zhang, Y.-Z., Wang, Y., Cheng, T., Yao, L.-Q., Li, X., Lai, W.-Y., et al. (2019). Printed Supercapacitors: Materials, Printing and Applications. *Chem. Soc. Rev.* 48, 3229–3264. doi:10.1039/C7CS00819H
- Zhang, G., Qin, P., Nasser, R., Li, S., Chen, P., and Song, J. (2020). Synthesis of Co(CO<sub>3</sub>)<sub>0.5</sub>(OH)/Ni<sub>2</sub>(CO<sub>3</sub>)(OH)<sub>2</sub> Nanobelts and Their Application in Flexible All-Solid-State Asymmetric Supercapacitor. *Chem. Eng. J.* 387, 124029. doi:10.1016/j.cej.2020.124029
- Zhang, X., Chen, P., Yang, F., Wang, L., Yin, J., Ding, J., et al. (2021a). Effect of FeCo<sub>2</sub>S<sub>4</sub> on Electrocatalytic I<sup>3-</sup> Reduction: Theoretical and Experimental Aspects. *Chem. Eng. J.* 424, 130419. doi:10.1016/j.cej.2021.130419
- Zhang, X., Li, D., Wang, L., Yang, F., and Wang, Y. (2021b). Induced Electron Transfer by Oxygen Vacancy Gradient on SnO<sub>2</sub> Conductive Glass for Electrocatalytic Reduction. *Sci. China Mater.* 64, 2081–2085. doi:10.1007/s40843-021-1674-3
- Zhou, J., Liu, Q., Feng, W., Sun, Y., and Li, F. (2015). Upconversion Luminescent Materials: Advances and Applications. *Chem. Rev.* 115, 395–465. doi:10.1021/cr400478f
- Zhu, R., Duan, H., Zhao, Z., and Pang, H. (2021). Recent Progress of Dimensionally Designed Electrode Nanomaterials in Aqueous Electrochemical Energy Storage. *J. Mater. Chem. A* 9, 9535–9572. doi:10.1039/D1TA00204J
- Zuo, X., Chang, K., Zhao, J., Xie, Z., Tang, H., Li, B., et al. (2016). Bubble-Template-Assisted Synthesis of Hollow Fullerene-Like MoS<sub>2</sub> Nanocages as a Lithium Ion Battery Anode Material. *J. Mater. Chem. A* 4, 51–58. doi:10.1039/C5TA06869J

**Conflict of Interest:** The authors declare that the research was conducted in the absence of any commercial or financial relationships that could be construed as a potential conflict of interest.

**Publisher's Note:** All claims expressed in this article are solely those of the authors and do not necessarily represent those of their affiliated organizations, or those of the publisher, the editors and the reviewers. Any product that may be evaluated in this article, or claim that may be made by its manufacturer, is not guaranteed or endorsed by the publisher.

Copyright © 2021 Duan, Shi, Zhang, Feng, Liu and Chen. This is an open-access article distributed under the terms of the Creative Commons Attribution License (CC BY). The use, distribution or reproduction in other forums is permitted, provided the original author(s) and the copyright owner(s) are credited and that the original publication in this journal is cited, in accordance with accepted academic practice. No use, distribution or reproduction is permitted which does not comply with these terms.